Deep-Sea Research, Vol. 33, No. 5, pp. 587–600, 1986.
Printed in Great Britain.

0198–0149/86 $3.00 + 0.00
Pergamon Journals Ltd.

Vertical electric field fluctuations at the floor of the Tasman Abyssal Plain

N. L. BINDOFF,* J. H. FILLOUX,† P. J. MULHEARN,‡ F. E. M. LILLEY* and I. J. FERGUSON*

(*Received* 14 *June* 1985; *in revised form* 25 *November* 1985; *accepted* 27 *November* 1985)

Abstract—A record of vertical electric field fluctuations occurring naturally in the ocean has been obtained at a site (36°14′S, 152°15′E) off the coast of eastern Australia, on the floor of the Tasman Abyssal Plain in water of depth 4836 m. The free-fall and self-contained sea-floor instrument measured ambient voltage fluctuations between two low-noise silver-silver chloride electrodes connected by a vertical insulated wire 160 m long. The record returned is 107 days in duration, with readings taken every 28⅛ s.

The data obtained are interpreted in terms of east–west fluid current motion past the wire, causing electromagnetic induction with the horizontal north component of the earth's steady magnetic field. These motional fields are observed on a wide range of time scales. Spectral analysis of the data shows inertial oscillations and shorter period internal waves, with good agreement between observation and the theory of CHAVE (1984, *Journal of Geophysical Research*, **89**, 10519–10528). There is also a peak in the power spectrum at the frequency of the semi-diurnal tides. The shortest period signals occurring are interpreted as due to some form of turbulence. Aperiodic motions on time scales of days are attributed to mesoscale activity in the East Australian Current system.

1. INTRODUCTION

THIS paper describes measurements of the vertical electric field at the sea floor, made over a period of 107 days as part of the Tasman Project of Seafloor Magnetotelluric Exploration (FERGUSON *et al.*, 1985; FILLOUX *et al.*, 1985; LILLEY *et al.*, 1986). The instrument, from the Scripps Institution of Oceanography in California, was deployed and retrieved by the Royal Australian Navy oceanographic ship HMAS *Cook*. The observations spanned the Universal Time period 12 December 1983–27 March 1984, at a site (TP6) on the Tasman Abyssal Plain off the coast of New South Wales at 36°14′S, 152°15′E in water of depth 4836 m (Fig. 1). The Tasman Abyssal Plain runs parallel to the Australian coast and bathymetric charts of the area, contoured at 500 m intervals, show the nearest contour to the west of site TP6 to be 4500 m at the foot of the Australian continental slope, some 100 km away. To the east of site TP6, the nearest contour (again 4500 m) occurs in conjunction with a region of seamounts, at distance 140 km. A sea-floor gradient of 1 in 300 is thus an upper limit for the Tasman Abyssal Plain in the region of the observing site, and at the time of deployment the echo-sounder of the ship was used to confirm that site TP6 was indeed flat and featureless.

* Research School of Earth Sciences, Australian National University, Canberra, ACT 2601, Australia.
† Scripps Institution of Oceanography, University of California, San Diego, La Jolla, CA 92093, U.S.A.
‡ Royal Australian Navy Research Laboratory, Darlinghurst, NSW 2010, Australia.

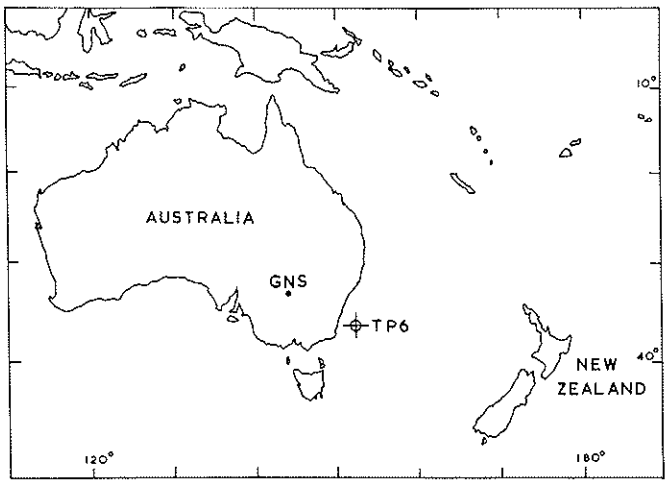

Fig. 1. Sea-floor site at 36°14′S, 152°15′E, where the vertical electric field (VEF) data described in the present paper were recorded. This site is denoted as site TP6 of the Tasman Project of Seafloor Magnetotelluric Exploration (TPSME). GNS denotes the land magnetometer station at Gunarremby Swamp, the data from which are used in the multiple coherence exercise in Section 5.1.

Although the physical principles involved are simple at the most basic level, the experimental procedures of sea-floor vertical electric field measurements are difficult and data are few. HARVEY (1972, 1974) reported a record of some 2.6 days duration of the vertical electric field measured off Hawaii, and showed it contained tidal and other signals. Also VEF records obtained with instrumentation similar to that of the present paper were obtained from other previous sea-floor magnetotelluric exercises (FILLOUX, 1981).

2. PHYSICAL PRINCIPLES

Electric fields are induced in the oceans by two physical mechanisms. The first mechanism is that of electromagnetic induction by time-varying source fields, which originate external to the earth. The second mechanism is that of ocean water motion in the earth's steady magnetic field. The analysis of these mechanisms is covered in the series of papers by LONGUET-HIGGINS *et al.* (1954), SANFORD (1971), LARSEN (1973), HARVEY *et al.* (1977), CHAVE (1983, 1984), and CHAVE and FILLOUX (1984).

For the horizontal electric field (HEF) signal at the sea floor the first mechanism (of ionospheric induction) is usually dominant; however, for the vertical electric field relatively little contribution is expected from this cause. The vertical electric field at the ocean floor may thus be considered to be almost purely of oceanic origin. Further, although the correct interpretation of the oceanic contribution to the HEF at the sea floor may need to be in terms of the motion of the whole water column, the VEF at the sea floor can be interpreted in terms of purely local east–west water motion. A VEF recording is thus in many respects similar to that produced by a mechanical current meter, except that a VEF signal is generated by the east–west (magnetic bearing) component of fluid flow only.

An advantage of VEF measurements is their high resolution. In the present experiment, with digital recording of the VEF signal, the digit of least count is equivalent to an east–west velocity of 4.0×10^{-2} cm s^{-1} in the local horizontal magnetic field of strength 23500 nT.

The basis of the theory in the present paper follows from STOMMEL (1948), who showed that motion of seawater in a magnetic field generates an electric field described by

$$\nabla\phi = \mathbf{v} \times \mathbf{B} - \mathbf{j}/\sigma, \tag{1}$$

where ϕ is the electrostatic scalar potential, $\mathbf{v}$ the velocity of the ocean, $\mathbf{B}$ the magnetic induction, $\mathbf{j}$ the electric current density and σ the electrical conductivity of the water. The motion is considered to be quasi-static so that the magnetic effects of self-induction and mutual induction can be ignored. We also assume that the magnetic field due to the induced electric currents is small when compared with the static magnetic field. It can be shown that the effect of induced electric fields on the moving ions is much smaller than the hydrodynamical forces in the fluid for current flows <1 m s^{-1} (SANFORD, 1971) and thus the water currents are largely unaffected by the motionally induced electric fields.

If the conductivity σ is uniform, using the relation

$$\nabla \cdot \mathbf{j} = 0 \tag{2}$$

it can be shown simply that,

$$\nabla^2\phi = \mathbf{B} \cdot \nabla \times \mathbf{v}. \tag{3}$$

This equation defines the potential for any arbitrary steady state velocity field.

By assuming the vertical electric current to be small and adopting a co-ordinate system of x to the horizontal magnetic north, y to the horizontal magnetic west, and z vertically upwards, equation (1) gives a vertical electric field value of

$$E_z = -\frac{\partial\phi}{\partial z} = v_y B_x. \tag{4}$$

Equation (4) thus expresses a direct linear relation between the east-to-west fluid velocity and the vertical electric field.

Because of the non-conductive atmosphere above the ocean, electric currents can not cross this interface, a situation which greatly contributes to the validity of the assumption of negligible vertical electric currents (i.e. $j_z/\sigma \ll v_y B_x$) in equation (1). Nevertheless, several oceanic processes may contribute to the generation of vertical electric currents and must be kept in mind when interpreting vertical oceanic electric field data. For instance baroclinic motions characterized by horizontal velocity fields with directions alternating with oceanic depth result in horizontal electric field components also alternating in direction, thus generating electric current circulation with vertical components. Although generally much less conducting than the ocean, the sea floor may also provide current return paths for electric fields that are uniform along the sea floor, as a consequence of the horizontal variability of oceanic velocity fields. Such a situation then leads to vertical electric current components, particularly in the vicinity of the sea floor. Thus the assumption of negligible vertical current depends critically on the scale and geometry of oceanic velocity fields, on the conductivity contrast between ocean and sea floor, and also on other factors such as irregularity of bathymetry, spatial variability of the magnetic field and to a lesser extent on seawater conductivity dependence on salinity

and temperature. It is, however, fortunate that many of the very different processes associated with vertical electric current contamination can be identified by characteristic features such as frequency bands of occurrence, correlation with other parameters, and precise process identification. An example of process identification is ionospheric induction at great distance from coastal boundaries, in which case all parameters are dominated by their horizontal expressions.

The recent contribution to this subject by CHAVE (1984) specifically analyses the electromagnetic fields induced by oceanic internal waves, and covers those cases where equation (4) becomes invalid. CHAVE (1984) also points out that severe ocean bottom topography may cause contamination of a VEF signal by an HEF signal, though the flat topography of site TP6 means this factor is unlikely to be important in the present case.

3. INSTRUMENTAL DETAILS

The VEF data of the present paper were recorded digitally on magnetic tape within the instrument, which lay moored at the sea floor. A schematic diagram of the instrument is shown in Fig. 2.

As in any electric field recording instrumentation to be used at sea the most satisfactory connection of the electric leads to the sea is made with well matched silver-silver chloride electrodes. Because of the highly specialized nature of this technique the reader is referred to FILLOUX (1973, 1974). Another component of the instrumentation requiring special attention is the electric cable whose strength must be high to sustain the

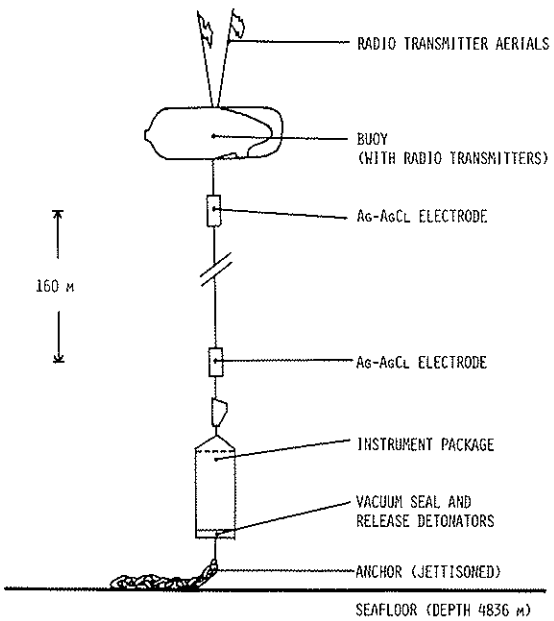

Fig. 2. Schematic diagram of the instrument used to record the vertical electric field data of the present paper. The buoy holds the insulated wire from the instrument package vertically upwards from the sea floor. At the end of recording the instrument package jettisons its anchor, and the buoy floats to the sea surface, lifting the cable and instrument package with it.

pull of a very buoyant float, yet which must contribute little current drag so as to ensure the best possible verticality.

The data sampling rate in the present experiment was 2^7 (=128) per hour, that is one reading every 28 s approximately, for the full recording period of 107 days. A unit increase in value of the least significant digit recorded is equivalent to a change in the potential difference of the upper electrode relative to the lower electrode of −1.51 μV. Since the electrodes are 160 m apart this change in potential difference is equivalent to an increase in the average upward electric field (defined as the negative gradient of potential) of +9.41 nV m^{-1}.

The effects of water motions with scale sizes less than or comparable to the electrode separation may thus be strongly attenuated in the data. As the electrode separation of 160 m spans the likely depth of an ocean-bottom boundary layer (Bird *et al.*, 1982), such attenuation may be expected to affect the VEF signal of boundary layer motions.

An order of magnitude estimate of the cable tilt for the present instrument can be made by considering the horizontal current drag on the float shown in Fig. 2. Following Harvey (1972) this drag is estimated to be <0.45 N for a water speed of 10 cm s^{-1}. The buoyancy force on the float is approximately 132 N, and cable tilt is thus estimated to be $<3 \times 10^{-3}$ rad. This small angle is not changed significantly by adding the drag on the cable, which may be of the same order as the drag on the float.

4. THE DATA OBSERVED

4.1 *The time series, and drift removal*

A plot of the basic data record, edited for imperfections in the tape recording process shows many important features (Fig. 3). Oscillations of approximately tidal periods (but of no obvious fixed phase) dominate the record, superimposed on an initially strong drift. There are times of high-frequency signal in the data.

To clarify the drift, a plot in Fig. 4 of 24 h averages (taken every 12 h) shows (a) the variations in the VEF with time scales of several days, and (b) the monotonic drift in the VEF during the whole recording period. This drift is considered to arise in the Ag-AgCl electrodes which make electrical connection with the seawater (Filloux, 1973, 1974). In the present study, the main drift contribution with time t (in days UT elapsed since 0000 h 1 December 1983) in the electric field E (in nV m^{-1}) between the electrode pair has been fitted empirically by a smooth monotonic function of form

$$E = a + bt + c \exp[-d(t - t_0)], \tag{5}$$

where a, b, c and d are arbitrary constants, and t_0 is the time of the first valid data point recorded by the VEF instrument. Time t_0 is known accurately. Fitting this expression to the data using non-linear least squares techniques results in

$$\begin{aligned} E = {} & (11464 \pm 149) + (97.7 \pm 1.9)t \\ & -(9537 \pm 364) \exp[(-0.20 \pm 0.014)(t - 11.56)] \end{aligned} \tag{6}$$

for the electrode drift in the data, where the errors quoted are standard error estimates.

A time series according to equation (6) has then been subtracted from the original data set, producing a new 'de-drifted' time series of hourly average values. These results (Fig. 5) suggest the absence of any substantial residual trend in the de-drifted data during the recording period. The most significant feature of Fig. 5, in addition to the effects with

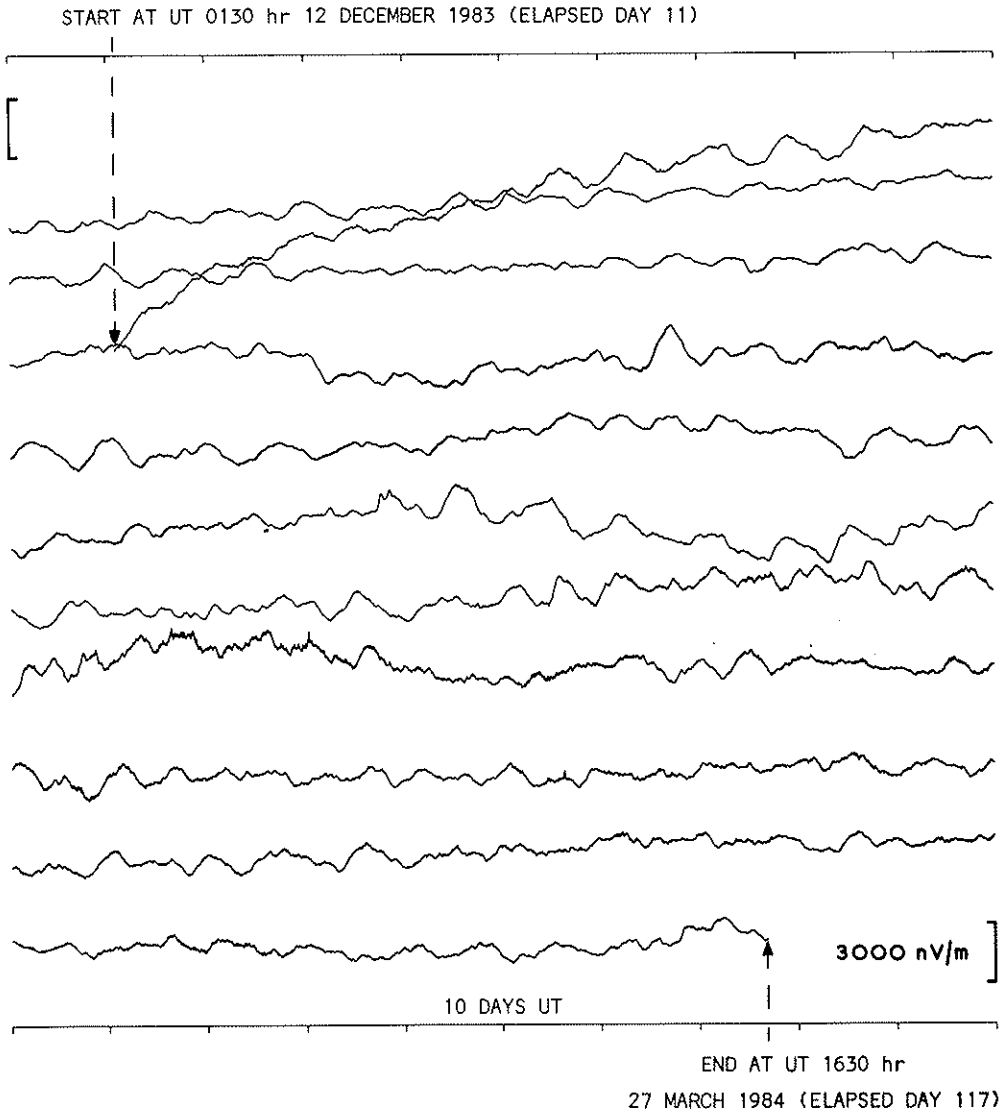

Fig. 3. Plot of the vertical electric field data at site TP6. The span of each full horizontal trace is 10 days of record, and the traces are consecutive from top to bottom of the figure. The two vertical scales, at the left-hand side of the top trace, and the right-hand side of the bottom trace, are each for an electric field change of 3000 nV m^{-1} corresponding to a velocity change, according to equation (4), of 12.8 cm s^{-1}. The trace going upwards in the diagram corresponds to the upper electrode voltage becoming more negative relative to the lower electrode, the upwards vertical electric field becoming more positive, and to the fluid velocity increasing in an east-to-west direction. The horizontal scales of the diagram are marked in days UT.

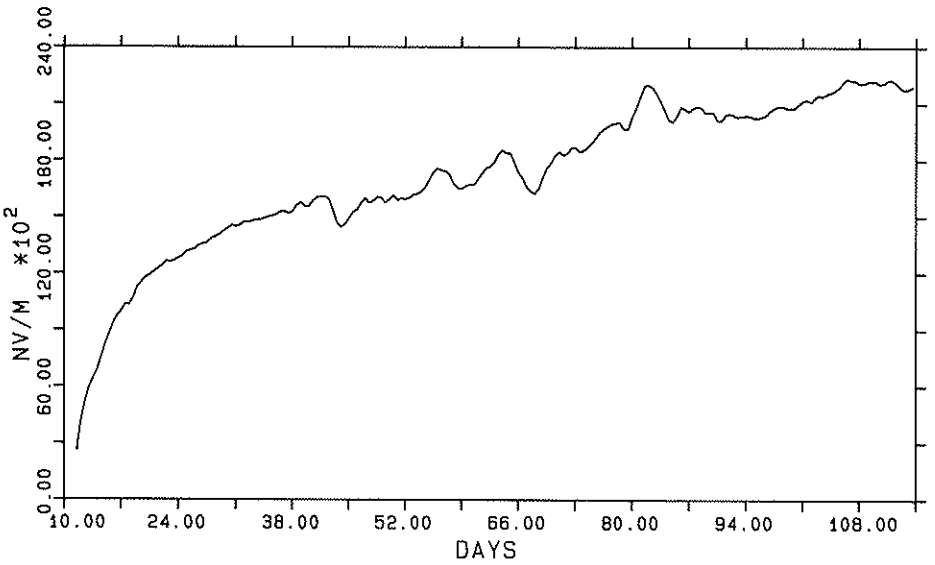

Fig. 4. Daily averages of the data of Fig. 3 compressed into a single plot. Time is marked as days UT elapsed from 0000 h 1 December 1983 (thus 1 December 1983 itself is day zero).

time scales of several days evident in Fig. 4, is the presence of oscillations of periods <1 day, which are present throughout the whole record.

4.2 *Spectral analysis*

A power spectrum was calculated for quarter-hourly averages of the de-drifted time series shown (as hourly average values) in Fig. 5. The power estimates were calculated

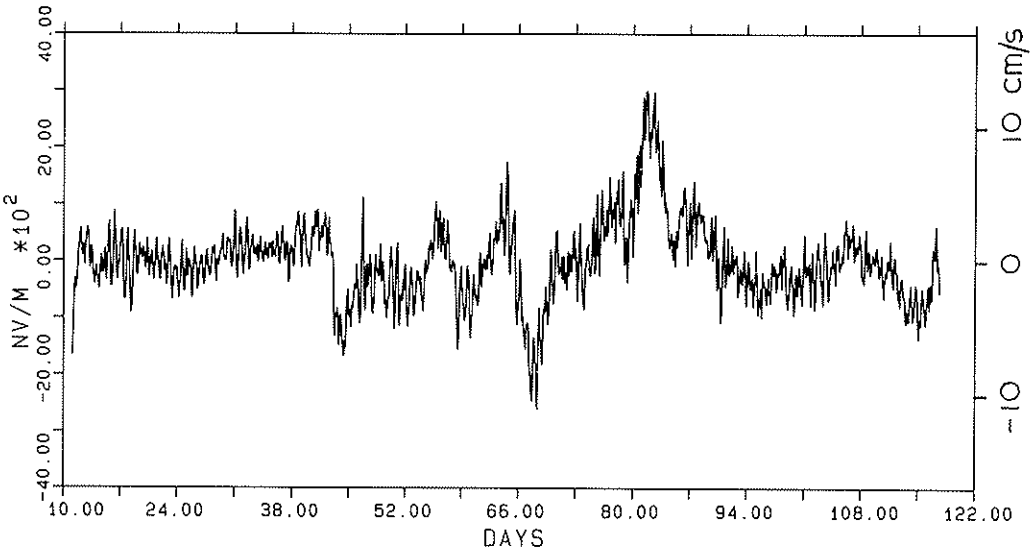

Fig. 5. Hourly averages of the 'de-drifted' VEF data set. Time scale is as for Fig. 4. The (east-to-west) velocity scale now included on the right-hand side of the figure is according to equation (4).

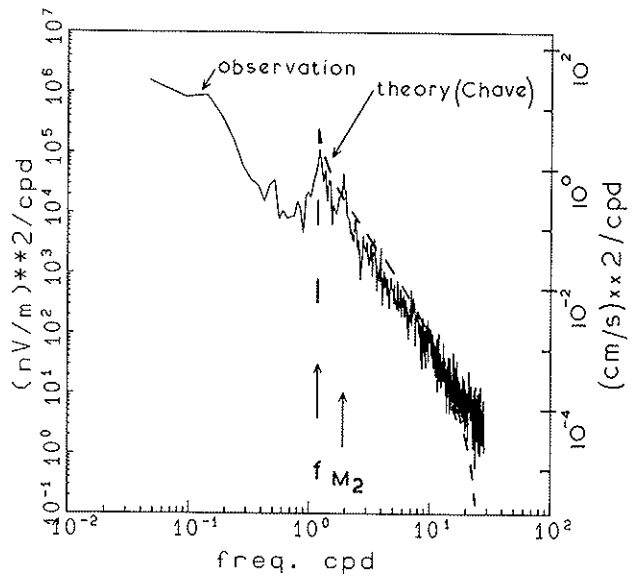

Fig. 6. Power spectrum for the de-drifted VEF data, on the basis of quarter-hour average values. The notations f and M_2 mark peaks identified as being due to inertial oscillations and semi-diurnal tides, respectively. The dashed line, with a sharp cut-off below the inertial frequency f, is for the internal-wave theory of CHAVE (1984) as discussed in Section 5.2. The scale in terms of velocity units on the right-hand side of the figure is based on equation (4), and may not apply when water motion is more complicated than as described there.

using a standard computing routine, which followed a procedure similar to Bartlett's Spectral Estimate (KANASEWICH, 1975, p. 99). The technique adopted divides a time series (padded as necessary with zeros which are subsequently corrected for) into m segments, each of which has L points, with no segment overlap. To take advantage of 'fast Fourier transform' techniques L is a power of 2, and tapering is applied to each segment using the symmetric window

$$W(j) = 1 - \frac{|j - (L-1)/2|}{|(L+1)/2|} \qquad j = 0, \ldots, L-1.$$

In the present case the original time series is of 10236 points and L is set as 2048, resulting in 10 d.f. for each power spectral estimate.

The power spectrum thus computed for the VEF data is shown in Fig. 6. The main features of this spectrum are: (a) the dominance of the low frequency component, for frequencies <0.2 cpd; (b) the two distinct peaks occurring, centred on periods of 19.7 and 12.5 hr; (c) the rapidly diminishing power (although linear on a log-log plot) at frequencies >0.5 cpd.

5. INTERPRETATION

Interpretation of the different phenomena recorded by the VEF instrument divides naturally into three ranges of time scale: <1 h; from 1 h to 1 day; and >1 day. These ranges of time scale will be discussed in turn.

5.1 *Signals with time scales* <1 h

Because quarter-hourly averages were used to compute the power spectrum of Fig. 6, the spectrum does not describe the high frequency content of the VEF data. However, the time series does contain some high frequency signals which occur intermittently with durations of days. An example (Fig. 7) shows two contrasting days taken from the de-drifted time series. The time scales of the high frequency signals typically are <1 h, and thus overlap with an estimated local buoyancy frequency for this site (~~2.5×10^{-4} Hz~~ or period ~~55~~ min). However, it is considered unlikely that the fluid motions causing these VEF signals are due to internal waves, since power spectral estimates predicted for such VEF signals are very low at or near the buoyancy frequency [e.g. CHAVE (1984) as discussed in Section 5.2.2).

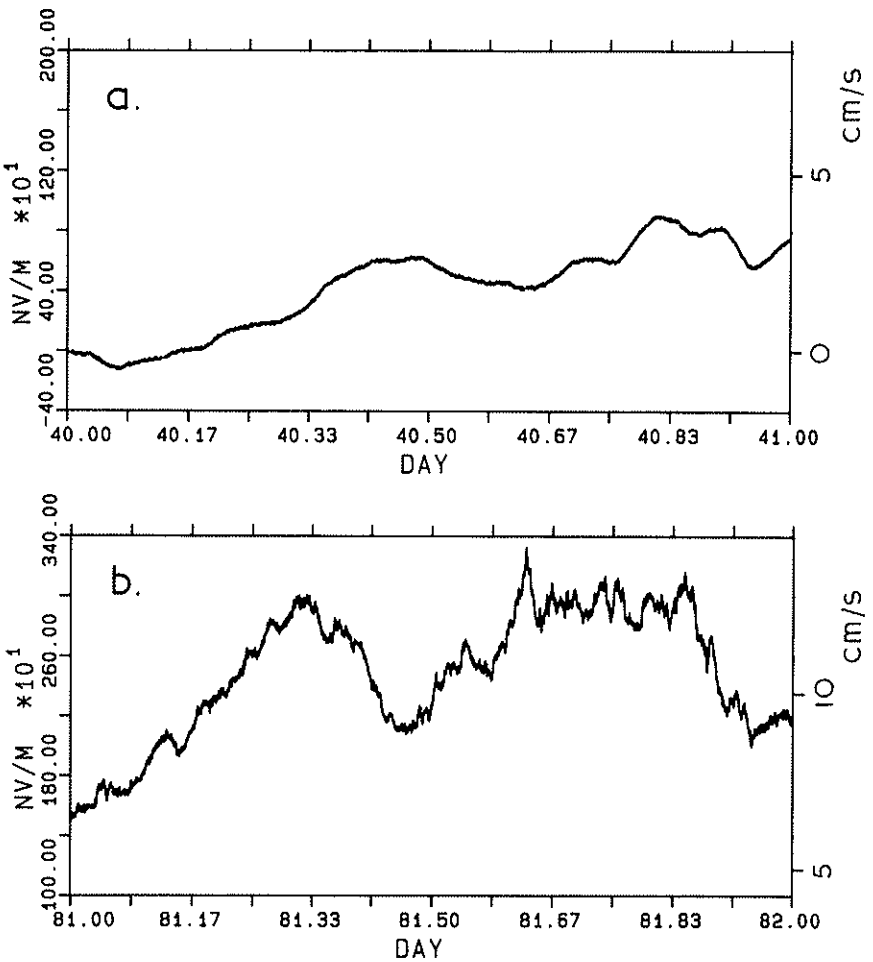

Fig. 7. Contrasting examples of 'quiet' and 'active' high frequency signals, interpreted as benthic boundary layer turbulence. (a) Day 40, a 'quiet' day, and one of low apparent mean velocity (~2 cm s^{-1}). (b) Day 81, an 'active' day, and one of high apparent mean velocity (~10 cm s^{-1}). The (east-to-west) velocity scale on the right-hand side of each figure is based on equation (4).

A possible mechanism for the high frequency signals observed may be benthic boundary layer turbulence. An estimate of the benthic boundary layer thickness (h) may be made using the relation

$$h = 1.3\, u_*/[f(1 + N_0^2/f^2)^{\frac{1}{2}}],$$

where u_* is the bottom friction current, f is the Coriolis parameter and N_0 is the buoyancy frequency (BIRD *et al.*, 1982). An estimate for u_* may be obtained using

$$u_* = u(C_0)^{\frac{1}{2}},$$

where u is the mean flow and is taken as 10 cm s^{-1} on day 81 (from Fig. 7b). Assuming a drag coefficient C_0 of 10^{-3}, u_* is thus estimated as 0.3 cm s^{-1}, and h as 47 m.

A time scale τ for such bottom boundary layer turbulence may be estimated using

$$\tau \sim h/u_* = 1.5 \times 10^4 \text{ s } (4.3 \text{ h}).$$

Thus the maximal time scale predicted for a bottom boundary layer mechanism with a thickness h of 47 m is of order 4 h, which is consistent with the observed data in Fig. 7b.

Further, by using the relation

$$E_0 = (1/\sqrt{3})B\, u_*$$

(COX *et al.*, 1970), where B is the total magnetic field (~59100 nT) and E_0 is the root-mean-square (r.m.s.) electric field, an estimate of the maximal r.m.s. electric field can be obtained. Using the above values, the maximum r.m.s. VEF in such a bottom boundary layer would be ~100 nV m^{-1}. This value is comparable to the high frequency signal evident in Fig. 7b, and demonstrates that bottom layer turbulence may have sufficient energy to account for the signal.

Another possible source of high frequency signal which should be considered is contamination of the VEF by HEF signals. Generally, such contamination could be produced either by a tilt of the VEF instrument cable away from a vertical orientation or by local topography tilting the HEF signal and thus producing a vertical component of the signal. For periods ranging from order 10 h to the shortest periods shown in Fig. 6, the HEF has sufficient power from induction by ionospheric sources (CHAVE and FILLOUX, 1984) such that small tilts could produce significant contamination of the VEF signal. A 1° tilt would be sufficient to produce significant contamination if at these periods the HEF has power two orders of magnitude greater than the VEF.

As a first test of the possibility of tilting, the squared multiple coherence of the VEF has been computed with the two horizontal components of magnetic fluctuations recorded simultaneously at land station GNS (33°16′S, 143°56′E, see Fig. 1). The data from this station (the furthest inland in the TPSME experiment) should provide a record of the ionospheric activity which also occurred above site TP6, but be free from any oceanographic effects.

Such a squared multiple coherence spectrum is shown in Fig. 8, calculated according to the discussion by CHAVE and FILLOUX (1984, p. 152) for two input signals. For the results in Fig. 8, segments of 4096 points at 3 min intervals have been taken using a Hanning window with no overlap. For the squared multiple coherence estimates below 3 cpd there are 22 d.f., between 3 and 30 cpd 88 d.f. and for >30 cpd 176 d.f.

In Fig. 8, the peak at 2 cpd (period 12 h) is interpreted as due to the near coincidence of the 12 h component in the general daily magnetic variation, and the semi-diurnal tidal

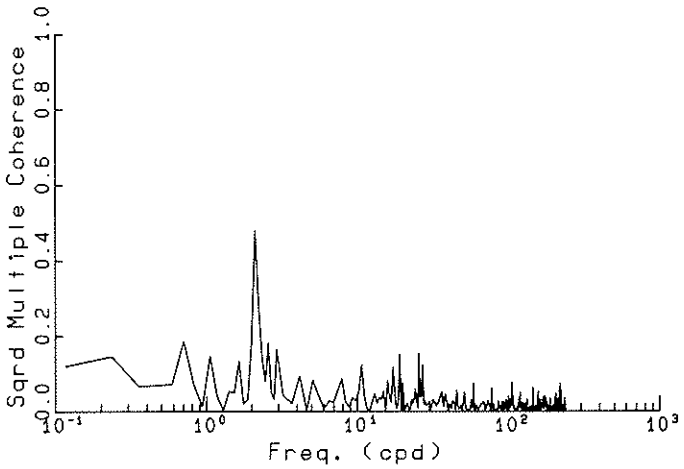

Fig. 8. Squared multiple coherence for the VEF signal at site TP6 with the two horizontal components of magnetic fluctuation recorded at inland magnetometer station GNS.

signal in the VEF data. Except for this peak the coherence in Fig. 8 is very weak. There is thus no indication that ionospheric source fields have contributed significant coherent power to the recorded VEF signal. More exhaustive tests would be required to examine the data for possible effects of time-varying cable tilt during the recording period, though the estimate of cable tilt in Section 3 indicates that maximum contamination of the VEF power spectrum due to cable tilt is –50 dB of the HEF power. Such a level of contamination is undetectable.

A similar exercise by CHAVE and FILLOUX (1985) with VEF data recorded near the crest of the East Pacific Rise shows, in contrast, a significant coherence of VEF with land magnetometer data. The present results (from a flat abyssal plain) suggest topographic contamination of the VEF by the HEF as an explanation of the Pacific Rise results. Such topographic contamination can arise from variations in sea-floor bathymetry, and also from lateral variations in the electrical conductivity structure of the sea-floor sediments and crust.

5.2 *Signals in period range* 1 h–1 day

Signals in the period range 1 h–1 day are shown most clearly by the power spectrum in Fig. 6.

5.2.1 *Inertial waves*. The dominant peak in the spectrum at 1.22 cpd (period 19.7 h) corresponds well to the inertial period of 20.3 h at the site latitude of 36°14′. Although the frequency resolution of the power spectrum shown in Fig. 6 is relatively low, the slightly shorter period observed for these inertial waves is consistent with results from deep-ocean current meters reported by FU (1981).

That inertial motions could appear in the energy spectrum of Fig. 6 is not unusual since current profiling by electromagnetic velocity profiler (SANFORD, 1975; SANFORD *et al.*, 1978) has demonstrated their energetic existence down to the greatest oceanic depths. In an attempt to evaluate the importance of these motions at the present site of observations, we have estimated that the energy in the inertial motion spectral peak roughly covers the interval 1.1–1.4 cpd, with an energy density around 10° $(\text{cm s}^{-1})^2$ or an

0.5 cm s^{-1} r.m.s. velocity for the east–west flow alone. The energy spectrum of Fig. 6 is similar in shape (though reduced numerically) to the results recorded by FU (1981) with conventional currents meters during POLYMODE, an experiment in the North Atlantic Ocean at a similar latitude.

5.2.2 *Internal waves.* Inertial waves may be regarded as being at one end of the range of ocean internal waves, and a spectrum for the VEF signal generated by internal waves is predicted by the theory of CHAVE (1984). In his paper, Chave uses the kinematic model of the internal wave field due to GARRETT and MUNK (1972). The general agreement of the Chave predictions with the observed spectrum in Fig. 6 accounts for much of the observed VEF signal at site TP6 in terms of internal waves.

5.2.3 *Tides.* The peak in the spectrum of Fig. 6 at a period of 12.5 h corresponds well with the semi-diurnal ocean tides. The resolution of the spectrum as computed is quite broad (0.04688 cpd between adjacent estimates at the tidal M_2 period) and thus other semi-diurnal tides (S_2, K_2 and N_2) are unresolved and all probably contribute to the single peak.

Diurnal tides do not appear to produce a distinct peak in the power spectrum of Fig. 6. This observation is consistent with other deep-ocean current meter data, for example, those of FU (1981) referred to above. While a relatively small peak at diurnal frequencies in the spectrum may be present but obscured by the strong inertial wave peak described above, the weakness of diurnal tide signal relative to semi-diurnal tide signal suggests that the latter is nearly an order of magnitude larger than the former at this site.

5.3 *Signals with time scales* >1 day

The signals in Figs 3–5 which have time scales of the order of several days are attributed to mesoscale motions in the ocean. The site of the present data lies in that part of the Tasman Sea where the East Australian Current flows over the Tasman Abyssal Plain, and eddies and fronts in the current are of fundamental importance to Australian oceanography. A comparison of the mesoscale VEF signals with a range of surface and near-surface measurements of the characteristics of the current is now being undertaken, with a view to its subsequent publication separately.

6. CONCLUSIONS

A range of oceanographic phenomena has been revealed by recording the vertical electric field at the deep-sea floor of the Tasman Abyssal Plain. The site is in a region which has very flat topography but which is within an active region of the East Australian Current. The range of the phenomena cover ocean floor turbulence, inertial waves, internal waves, tides, and mesoscale motions.

The power spectrum of the VEF data has spectral peaks for tides and inertial oscillations which are similar (though of generally reduced energy) to conventional current meter data measured in deep oceans. Over the internal wave band of frequencies, the observed VEF spectrum agrees well with the predictions of CHAVE (1984). The sensitivity of the VEF instrument has enabled the detection of east–west ocean-bottom currents with energy densities as low as 10^{-3} or 10^{-4} $(\text{cm s}^{-1})^2$/cpd, associated with internal waves.

Acknowledgements—The TPSME experiment, of which the present paper reports one part, was made possible by the support of the Royal Australian Navy oceanographic vessel HMAS *Cook* for two cruises, in December 1983 and March/April 1984. We thank particularly the ship's company for their skillful deployment and retrieval of the instrument, and for their hospitality to us while on board ship. H. Moeller, G. Pezzoli and T. Koch of the Scripps Institution of Oceanography were essential members of the experimental team. The project was run under the U.S.–Australia Agreement for Science and Technology, and U.S. participation was supported by National Science Foundation grants OCE 83-01216 and OCE 83-12339.

At the Australian National University, the encouragement and interest in the project of A. L. Hales, K. Lambeck, A. E. Ringwood, and J. S. Turner has been much appreciated, and we have benefited from discussions on the data with R. W. Griffiths. At Scripps Institution of Oceanography, we thank A. D. Chave in particular for his contribution of the theoretical curve plotted in Fig. 6. N.L.B. and I.J.F. are the recipients, respectively, of an Australian Commonwealth Postgraduate Research Award and an Australian National University Postgraduate Scholarship.

REFERENCES

Bird A. A., G. L. Weatherly and M. Wimbush (1982) A study of the bottom boundary layer over the eastward scarp of the Bermuda Rise. *Journal of Geophysical Research*, **87**, 7941–7954.

Chave A. D. (1983) On the theory of electromagnetic induction in the earth by ocean currents. *Journal of Geophysical Research*, **88**, 3531–3542.

Chave A. D. (1984) On the electromagnetic fields induced by oceanic internal waves. *Journal of Geophysical Research*, **89**, 10519–10528.

Chave A. D. and J. H. Filloux (1984) Electromagnetic induction fields in the deep ocean off California: oceanic and ionospheric sources. *Geophysical Journal of the Royal Astronomical Society*, **77**, 143–171.

Chave A. D. and J. H. Filloux (1985) Observation and interpretation of the seafloor vertical electric field in the eastern North Pacific. *Geophysical Research Letters*, **12**, 793–796.

Cox C. S., J. H. Filloux and J. C. Larsen (1970) Electromagnetic studies of ocean currents and electrical conductivity below the ocean-floor. In: *The sea*, Vol. 4, A. E. Maxwell, editor, Wiley Interscience, New York, pp. 637–693.

Ferguson I. J., J. H. Filloux, F. E. M. Lilley, N. L. Bindoff and P. J. Mulhearn (1985) A seafloor magnetotelluric sounding in the Tasman Sea. *Geophysical Research Letters*, **12**, 545–548.

Filloux J. H. (1973) Techniques and instrumentation for study of natural electromagnetic induction at sea. *Physics of the Earth and Planetary Interiors*, **7**, 323–338.

Filloux J. H. (1974) Electric field recording on the seafloor with short span instruments. *Journal of Geomagnetism and Geoelectricity*, **26**, 269–279.

Filloux J. H. (1981) Magnetotelluric exploration of the North Pacific: progress report and preliminary soundings near a spreading ridge. *Physics of the Earth and Planetary Interiors*, **25**, 187–195.

Filloux J. H., F. E. M. Lilley, I. J. Ferguson, N. L. Bindoff and P. J. Mulhearn (1985) The Tasman Project of Seafloor Magnetotelluric Exploration. *Exploration Geophysics*, **16**, 221–224.

Fu L. (1981) Observations and models of inertial waves in the deep sea. *Reviews of Geophysics and Space Physics*, **19**, 141–170.

Garrett C. J. R. and W. H. Munk (1972) Space-time scales of internal waves. *Geophysical Fluid Dynamics*, **3**, 225–264.

Harvey R. R. (1972) Oceanic water motions derived from the measurement of the vertical electric field. Report HIG-72-7, Hawaii Institute of Geophysics, University of Hawaii, Honolulu.

Harvey R. R. (1974) Derivation of oceanic water motions from measurement of the vertical electric field. *Journal of Geophysical Research*, **79**, 4512–4516.

Harvey R. R., J. C. Larsen and R. Montaner (1977) Electric field recording of tidal currents in the Strait of Magellan. *Journal of Geophysical Research*, **82**, 3472–3476.

Kanasewich E. R. (1975) *Time sequence analysis in geophysics*, 2nd edition, University of Alberta Press, 364 pp.

Larsen J. C. (1973) An introduction to electromagnetic induction in the ocean. *Physics of the Earth and Planetary Interiors*, **7**, 389–398.

Lilley F. E. M., P. J. Mulhearn, J. H. Filloux, N. L. Bindoff and I. J. Ferguson (1986) Pressure fluctuations on the open-ocean floor: mid-Tasman Sea at 38°30′S, 162°38′E, near the Lord Howe Rise. *Australian Journal of Marine and Freshwater Research*, **37**, 27–37.

Longuet-Higgins M. S., M. E. Stern and H. Stommel (1954) The electric field induced by ocean currents and waves, with applications to the method of towed electrodes. Papers in Physical Oceanography and Meteorology published by MIT and Woods Hole Oceanographic Institution, Vol. XIII, No. 1, pp. 1–37.

Sanford T. B. (1971) Motionally induced electric and magnetic fields in the sea. *Journal of Geophysical Research*, **76**, 3476–3492.

SANFORD T. B. (1975) Observations of vertical structures of internal waves. *Journal of Geophysical Research*, **80**, 3861–3871.

SANFORD T. B., R. G. DREVER and J. H. DUNLAP (1978) A velocity profiler based on the principles of geomagnetic induction. *Deep-Sea Research*, **25**, 183–210.

STOMMEL H. (1948) The theory of the electric field induced in deep ocean currents. *Journal of Marine Research*, **7**, 386–392.